Issues in Simulating the Annual Precipitation of a Semiarid Region in Central Spain

N. HASLER AND R. AVISSAR

Department of Civil and Environmental Engineering, Duke University, Durham, North Carolina

G. E. LISTON

Department of Atmospheric Science, Colorado State University, Fort Collins, Colorado

(Manuscript received 24 March 2004, in final form 5 November 2004)

ABSTRACT

Running regional climate models at a high resolution may improve their ability to simulate regional precipitation patterns, making them suitable for studying the impact of human-induced land-cover changes on hydrometeorology. The performance of the Regional Atmospheric Modeling System (RAMS) run in the high-resolution climate mode (4-km grid mesh) has been tested over a small domain in a semiarid region in central Spain. Three 1-yr simulations representing dry, intermediate, and wet conditions were compared to observations collected in 35 rain gauges. The model captured general spatiotemporal features of precipitation, such as the timing of precipitation events and approximate location of storms. A high correlation (0.82) between monthly domain-averaged observed and modeled precipitation was obtained. However, the model had a systematic dry bias, averaging -0.29 mm day^{-1}, equivalent to 26% of annual rainfall. The small domain size, chosen because of computational limits, induced strong lateral boundary forcing, which, combined with uncertainty in NCEP relative humidity fields, was a likely cause for this dry bias.

1. Introduction

Land-cover change is a significant cause of climate perturbation (e.g., Avissar and Verstraete 1990; Dickinson 1995; Sellers et al. 1997; Houghton et al. 2001; Pielke 2001; Marland et al. 2003). Assessing the potential impact of human-induced land-cover changes on the climate system has been preformed with general circulation model (GCM) sensitivity experiments (Shukla and Mintz 1982; Dickinson and Henderson-Sellers 1988; Betts et al. 1996; Werth and Avissar 2002). Although GCMs provide the global and long-term features required for climate studies, their spatial resolution is too coarse to be directly applied at the regional scale (Houghton et al. 2001). Their resolution is also generally too coarse to capture land-generated mesoscale circulations. On the other hand, limited-area models (LAMs) provide a better representation of the regional meteorology, but have much higher computational costs. Therefore, most investigations of the potential impact of human-perturbed lands on the climate system with LAMs have been limited to short time scales and specific regional meteorological situations, lasting from a single day to a couple of months (Segal et al. 1988; Segal and Arritt 1992; Weaver and Avissar 2001; Baidya Roy et al. 2003a). Though limited in time, these research efforts largely improved our general understanding of land surface–atmosphere processes and feedbacks (Pielke 2001). Yet the long-term evolution of these regional processes and feedbacks still needs to be explored.

Dickinson et al. (1989) and Giorgi (1990) first investigated the use of LAMs for regional climate studies. In an early effort, Giorgi and Bates (1989) preformed a one-month-long simulation using GCM output as lateral boundary conditions for a high-resolution LAM, demonstrating that long duration, continuous simulations are possible. Expansion to multiyear regional nested simulations was then conducted by Giorgi et al. (1993) and Jones et al. (1995) and has since been performed with many models for a variety of applications. Hydrologic fluxes and states are consistently the most improved fields in regional, as compared to global, climate simulations.

While increasingly used in regional climate settings, LAMs [called in this context regional climate models (RCMs)] suffer from a few drawbacks, most of which are already present in short-term simulations for weather predictions (Warner et al. 1997). Their needs for lateral boundary condition introduce direct and in-

Corresponding author address: Roni Avissar, Department of Civil and Environmental Engineering, Edmund T. Pratt Jr. School of Engineering, 123 Hudson Hall, Duke University, Durham, NC 27708-0287.
E-mail: avissar@duke.edu

direct problems such as the quality and frequency of the data, the mismatch of resolution between the model and this data, domain size, "buffer" width, and data nesting technique [see reviews of Giorgi and Mearns (1999) and Denis et al. (2002) for more details on these issues]. Separating errors due to RCM formulation from errors imported in the model from forcing data is a challenging aspect of RCM validation (Christensen et al. 2001; Caya and Biner 2004). One way of evaluating the accuracy of the model physics, as separate from the accuracy of the forcing data, is to perform an ensemble of simulations with different models forced with the same conditions. This approach was employed in the Project to Intercompare Regional Climate Simulations (PIRCS; Takle et al. 1999), which assessed the capability of eight different atmospheric mesoscale models to simulate climate, including the Regional Atmospheric Modeling System (RAMS; Pielke et al. 1992; Cotton et al. 2003). Two-month experiments, performed for the continental United States, showed that variability between RCMs was as large as interannual variability between summers of drought and flood years. They also showed that for all models, organized synoptic-scale precipitation systems were more accurately simulated than scattered convective precipitation.

Most published experiments with RCMs (including PIRCS) have been performed with a grid-mesh size of about 50 km, requiring parameterization of convective precipitation. Whether higher resolution would improve the representation of the regional climate system remains to be assessed. Since circulations induced by land surface features, often associated with convection, occur preferentially at 10–20-km length scales (Baidya Roy et al. 2003b), finer resolution may be particularly important in studies of land-cover change impacts on climate.

Convection is an important atmospheric process characteristic of the western Mediterranean semiarid summers. Precipitation in the region exhibits strong seasonality and significant interannual variability (Bolle et al. 1993). Previous studies report that the region's climate is the most sensitive of those in Europe to land surface processes (Heck et al. 2001) and has already experienced changes associated with land-cover modifications (Reale and Shukla 2000; Gaertner et al. 2001; Heck et al. 2001). High sensitivity was attributed to the frequent occurrence of high pressure systems associated with weak large-scale advection into the region, allowing convection buildup. Provided the importance of convection in the region, and known limitations of representing the convective process with a coarse resolution, it is likely that a high-spatial-resolution model will better reproduce observed precipitation patterns and improve the representation of climate sensitivity to land-cover change.

The purpose of this study is to evaluate the performance of RAMS (Pielke et al. 1992; Cotton et al. 2003) setup in a high-resolution climate mode for the semiarid area of central Spain. Its capability to reproduce seasonally evolving precipitation is tested over this region for different climatological situations (dry, intermediate, and wet). The model is tested for reliability in simulating precipitation timing, magnitude, and spatial distribution.

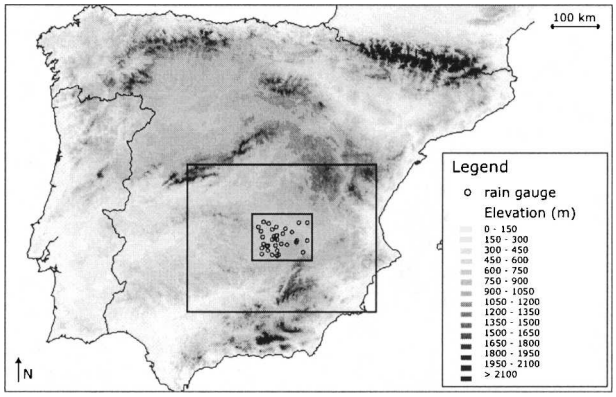

FIG. 1. The two nested grids used for the model evaluation (solid rectangles) and location of the 35 rain gauges (dots).

In what follows, the main characteristics of the study area are described, the model and the simulations are presented, and a sensitivity study of the key model parameters is provided.

2. Study area

The study area (128×96 km^2) is located in Castilla-La Mancha (central Spain), characterized by elevated flat lands (700–800 m) surrounded by mountains (Figs. 1 and 2). It is a complex landscape consisting of forested areas, shrublands, semidesertic vegetation, irrigated and nonirrigated fields, and traditional agro-silvo-pastoral farmlands (called *dehesa*) comprised of an openly spaced evergreen woodland—usually oaks—overlying a grass or crop layer. The climate of Spain is Mediterranean, representing a high level of continentality, but influenced by westerlies from the Atlantic Ocean. It is at a latitudinal transition between midlatitude low pressure areas and the subtropical highs (Romero et al. 1999). Rain distribution throughout the year is directly linked to the Azores high, and the main disturbances are linked to the jet stream and the polar-front patterns (Rodrigo et al. 1999). It presents strong seasonal contrasts with particularly dry summers, and significant interannual precipitation variability (Bolle et al. 1993). In summertime, the displacement of the polar front to higher latitudes usually leads to weak synoptic-scale activity, allowing thermally induced mesoscale systems to develop. The most typical surface meteorological pattern corresponds to a well-developed thermal depression, almost centered on the Iberian Peninsula, known as the Iberian thermal low (Gaertner et al. 1993). Over Castilla-La Mancha, large-

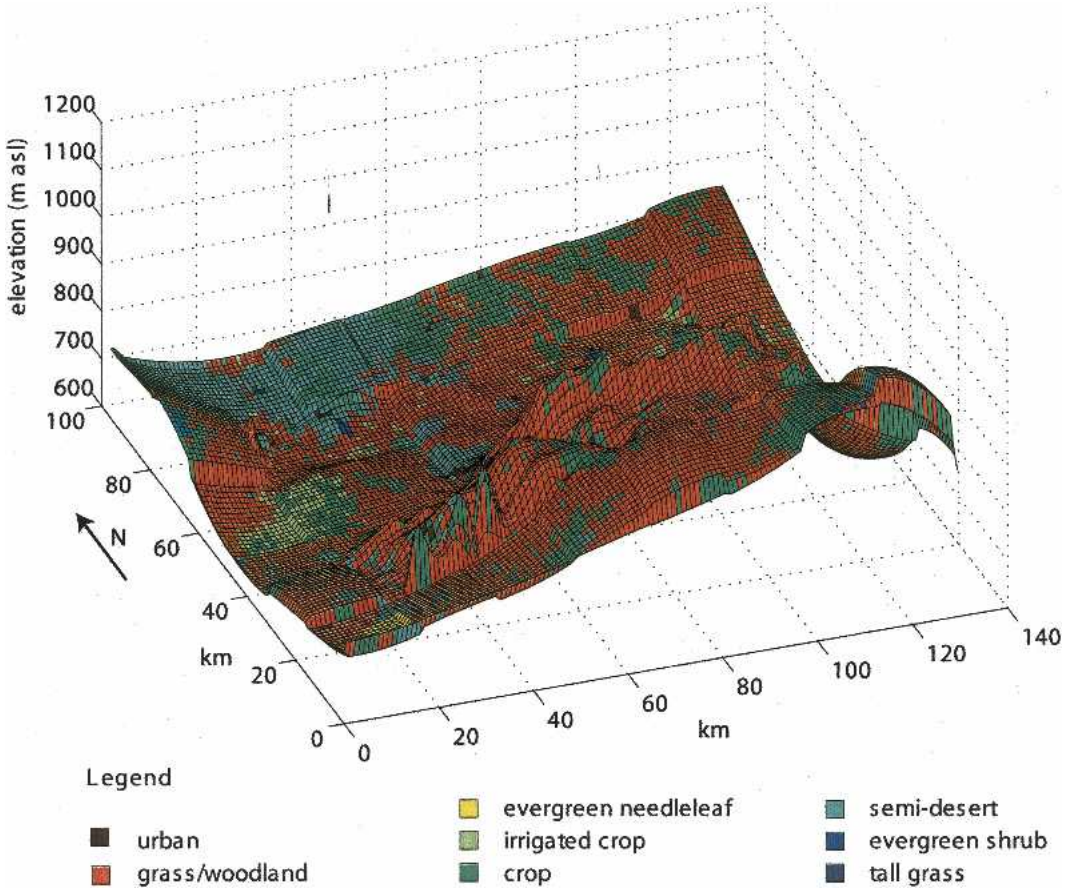

FIG. 2. Land-cover types and elevation of the 4 km × 4 km simulated grid.

scale precipitation, occurring mostly in spring and fall, is linked to Atlantic and Mediterranean influences, while summertime (May to September) precipitation is largely convective. Mean annual precipitation is approximately 400 mm yr^{-1}, with 50–80 days of rainfall each year (Garcia de Pedraza and Rieja Garrido 1994).

3. Numerical experiment

a. Model

RAMS version 4.4 is used for this study. This model solves the nonhydrostatic equations of motion, heat, moisture, and mass continuity, in a σ_z terrain-following coordinate system and has telescoping, two-way interactive grid-nesting capability. The Chen and Cotton (1987) radiation scheme was adopted here. Turbulence is parameterized with the Mellor and Yamada (1982) ensemble closure scheme. RAMS uses a nudging technique based on Davies (1983) for its lateral boundaries, and it computes the surface layer fluxes of heat, momentum, and water vapor according to Louis (1979).

Subgrid-scale land–atmosphere exchanges (and storage) of heat and moisture is parameterized with the Land Ecosystem–Atmosphere Feedback model version 2 (LEAF-2; Walko et al. 2000), where the land surface consists of a "mosaic of tiles" (Avissar and Pielke 1989). Each tile consists of a vegetation layer over a multilayer soil profile or, alternatively, a body of water. Prognostic temperature and moisture variables are computed for bare soil (McCumber and Pielke 1981; Tremback and Kessler 1985) and vegetation (Lee 1992) by solving the surface energy and water balance equations while accounting for vertical diffusion in the soil. A zero flux condition is imposed at the lower boundary (i.e., the deepest soil layer set at 2 m here). Modeled land surface characteristics are provided by the 30 arcsecond (approximately 1 km) resolution Global Topographic dataset (GTOPO30; data and references can be found online at edcdaac.usgs.gov/gtopo30/gtopo30.html) and the 2.0 version of the 1-km resolution Global Land Cover Characteristics (GLCC) database (data and references can be found online at edcdaac.usgs.gov/glcc/glcc.html). Vegetation and soil characteristics are provided for 30 land-cover classes and 11 soil textural classes (Walko et al. 2000).

RAMS uses a modified scheme of the generalized form of the Kuo (1974) convective parameterization to

TABLE 1. Simulations' setup.

Condition	Value
Simulation periods	15 months: Oct–Dec. Years 1991–92, 1993–94, and 1996–97 selected as intermediate, dry, and wet years, respectively.
Atmospheric lateral boundary conditions	NCEP 6-hourly reanalysis data
Current land cover	GLCC—1-km resolution, version 2.0
Elevation	GTOPO30—30 arc-second resolution
Soil texture	Uniform sandy clay loam
Initial soil moisture	Constant profile at 50% of saturation value
Center of the domain	39.11°N, 2.85°W
Center of projection	At center of domain (39.11°N, 2.85°W)
Horizontal grids	Grid 1: 26 × 20 elements, 16 km × 16 km each Grid 2: 34 × 26 elements, 4 km × 4 km each
Vertical resolution	42 levels in σ_z terrain-following coordinates, with first z at 30 m and a stretch of 1.1 (max depth allowed 1000 m)
Top of the model	21 371 m
Nudging condition	Davies (1983) flow relaxation scheme on the five outer grid cells of the coarse grid
Precipitation scheme	Modified Kuo (1974) convective parameterization scheme on coarser grid, and full microphysics on all grids.
Turbulence closure	Mellor and Yamada (1982)
Surface layer	Louis (1979) and Walko et al. (2000)
Radiation scheme	Chen and Cotton (1987)

account for convection-produced precipitation (Molinari 1985). It also explicitly solves cloud and precipitation microphysics (Walko et al. 1995; Meyers et al. 1997). Each water category (cloud water, rain, pristine ice, snow, aggregates, graupel, and hail) is treated as a generalized gamma distribution, with specified growth characteristics, transformation for one category to another, and differential fall speeds (except for cloud water, which does not fall). The autoconversion of cloud droplets to rain is based on a threshold average diameter in the droplet distribution. The hydrometeor heat budget equations include sensible heat transfer in interspecies collisions. Both convective parameterization and microphysics can be used jointly or individually on each grid independently.

b. Simulation setup

Because of high computational cost of combining high-resolution and long-term simulations, only a small 416 km × 320 km domain centered at 39.11°N, 2.85°W could be selected for the numerical experiments (see Figs. 1 and 2 and Table 1). This area was represented by a grid in the RAMS polar stereographic projection using 26 × 20 elements, each 16 km × 16 km. A high-resolution grid of 34 × 26 grid elements, each 4 km × 4 km, was nested in the center of this coarser grid. Both grids had 42 vertical levels with the lowest one being 30 m deep and with a stretching factor of 1.1 above. Thus, the top of the domain reached a height of 21 370 m. While full microphysics was used on both grids to simulate clouds and precipitation, the Kuo (1974) convective parameterization was used only on the coarser grid.

To account for interannual variability in precipitation, simulations were performed for three different years. Based on 1981–2001 precipitation time series for this region (see Fig. 3), 1994 and 1997 were selected as dry and wet years, respectively. In addition, 1992 was chosen as an *intermediate* year, as annual precipitation in 1992 was close to the mean annual precipitation from the 20-yr record. A three-month spinup period was added to each run by starting the simulation on 1 October of the prior year. The results from the spinup period were eventually discarded and not used for our analysis.

Because of the lack of reliable soil data, an idealized uniform 2-m-deep sandy clay loam soil was initially moistened at 50% of saturation value. The soil temperature was initialized with a 0- to 5-K offset of initial air temperature. While these conditions were selected in agreement with previous measurements and findings (Braud et al. 1993; Braud et al. 2003; Miao et al. 2003; Jochum et al. 2004), the three-month spinup period during the rainy season was intended to allow the

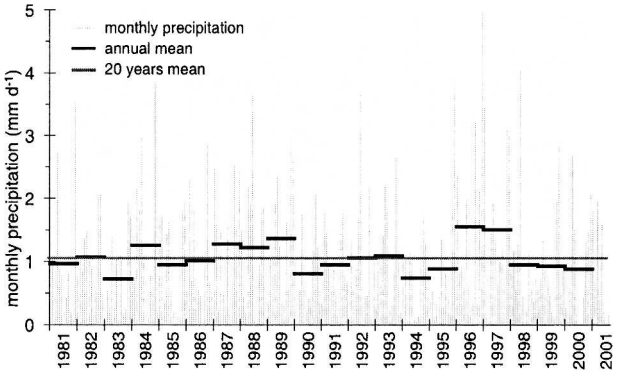

FIG. 3. Monthly precipitation time series in the simulated region.

model to adjust to the initial conditions. Liu and Avissar (1999a,b) indicated that soil moisture in semiarid areas has a persistence of about three months, and this spinup period was defined accordingly. Sensitivity to these idealized conditions is evaluated in section 5.

Atmospheric initial and lateral boundary conditions, consisting of 6-hourly air temperature, horizontal wind components, relative humidity, and geopotential height, were provided by the 17 pressure levels, global 2.5° × 2.5° latitude–longitude National Centers for Environmental Prediction (NCEP) reanalysis data. The variables were nudged over the five outer-boundary grid cells of the coarse grid and interpolated in time and space. Table 1 summarizes the model structure used in this study.

4. Model evaluation

a. Observation datasets and evaluation method

Observed precipitation data were obtained from the Spanish Meteorological Center [Instituto Nacional de Meteorología (INM)]. These data come from a volunteer-based network of 35 rain gauges, all located within the research area and referred to here as the "gauge" data. The choice of gauges was made to maximize the spatial coverage while minimizing missing data. Only 24 stations out of the 35 had data for 1994, and 34 out of 35 for 1997. The selected rain gauges were compared to the four INM meteorological stations closest to the study region (each one is located within 30–50 km from a different corner of the domain) and are referred to here as the "INM" data. The spatial average of the gauge monthly precipitation highly correlated with the average of monthly INM data (1992: $r = 0.94$, 1994: $r = 0.91$, 1997: $r = 0.79$). Gauge annual precipitation differed from the INM data by 0.09, −0.25, and −0.33 mm day^{-1}, representing 8%, 38%, and 22% of the annual precipitation for 1992, 1994, and 1997, respectively. The average gauge data were generally in the range defined by the four INM stations, indicating overlap and general agreement despite the large spatial variability. This comparison shows magnitude of differences found between two independent datasets supposedly representative of the region of interest.

Modeled precipitation was bilinearly interpolated to the gauge locations for site-specific comparisons. Monthly precipitation biases and absolute values of the difference between simulated and observed monthly precipitation were calculated on a station-by-station basis. Subjective criteria were defined to test the model performance. Given known errors in rain gauge data, considered to range between 0% and 15% (Bruce and Potter 1957; Sevruk 1982) or even 40% (Legates and Deliberty 1993) of the corresponding precipitation value in average and to vary from 0% to 75%, a 0%–30% bias between model and observation was subjectively chosen as a "reasonable" match. Error for small storms can exceed several hundred percent (Neff 1977); thus a 0.11 mm day^{-1} monthly bias was allowed as a complementary lower bound. This threshold value was obtained by calculating the mean bias between gauge and INM data for monthly precipitation lower than 0.3 mm day^{-1}. Thus, the model was considered to agree with observations when one of the following conditions was satisfied: (a) the bias was smaller than 0.11 mm day^{-1}; (b) the bias was lower than 30% of the observed value; or (c) the mean of the absolute value of the differences was less than or equal to the spatial standard deviation of the observations. The latter conditions attempt to evaluate the goodness of fit with respect to the degree of spatial variability in rainfall, similar to Keyser and Anthes (1977). In addition to those criteria, correlation, root-mean-square error (rmse), and precipitation threat score were calculated and analyzed (Wilks 1995). The threat scores were calculated for different precipitation thresholds, indicative of the spatial accuracy of simulated monthly rainfall exceeding each threshold.

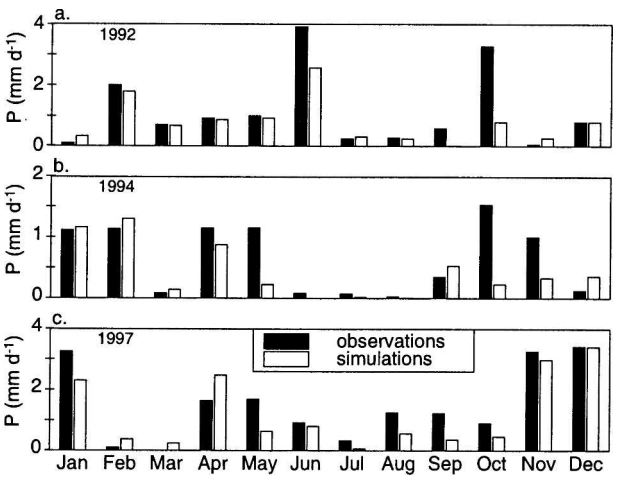

FIG. 4. Monthly precipitation (mm day^{-1}) averaged for the 35 rain gauges (black bars), and the corresponding 35 spatially averaged, 4-km-grid simulated values interpolated to the gauge locations (white bars) for (a) 1992, (b) 1994, and (c) 1997.

b. Average monthly precipitation

Figure 4 shows monthly rainfall for the three simulation years for both the spatial average of the 35 gauge records (observed) and the spatial average of the 35 simulation records, obtained from the bilinear interpolation of the 4-km grid. Table 2 shows the mean monthly statistics, and Table 3 details the monthly agreement criteria. Overall, modeled monthly rainfall was 0.29 mm day^{-1} lower, or 26% less, than observed monthly rainfall when averaged over the 35 stations and the three years. Modeled monthly rainfall was strongly correlated with that observed when both were averaged over the domain ($r = 0.82$, $n = 36$). Mean monthly root-mean-square errors were lower than the

TABLE 2. Statistics of the simulated and observed monthly precipitation at the 35 rain gauge locations, provided by bias, rmse, standard deviation, and correlation coefficients. The domain correlation coefficient (DCC) is the correlation coefficient between the average of the 35 rain gauge observed values, and the corresponding 35 averaged 4-km-grid simulated values ($n = 12$), while the stations' correlation coefficient (SCC) is the correlation coefficient between observed and simulated monthly precipitation rates at each station location ($n = 420$, 288, 408 for 1992, 1994, 1997, respectively).

	1992	1994	1997
Bias (mm day^{-1})	−0.36	−0.22	−0.28
Rmse (mm day^{-1})	1.01	0.65	0.86
DCC	0.80	0.54	0.89
SCC	0.68	0.44	0.79
Obs std dev (mm day^{-1})	1.29	0.66	1.28

mean monthly observed standard deviation, for every simulated year. The defined agreement criteria were satisfied by 27 of the 36 simulated months, or 75% of the cases. The accuracy differed depending on the season. While winter months, from December to April, matched better the observations, differences increased in spring and fall. The model was also able to reproduce the dry condition of July–August summer months. For the year representing intermediate rainfall conditions, 1992, modeled and observed monthly values and trends agreed very well ($r = 0.8$, $n = 12$), except for June, September, and October. The average bias was −0.36 mm day^{-1}, decreasing to −0.05 mm day^{-1} (7% bias) when discarding June and October. The dry year, 1994, had a small bias (−0.22 mm day^{-1}) due to small precipitation amounts. The 0.54 domain-averaged correlation coefficient showed the model difficulty to reproduce the relatively strong annual cycle of that year. Similar to 1992, May, October, and November 1994 were poorly reproduced by the model. The mean bias for 1997 (−0.28 mm day^{-1}, representing 18% of the observed precipitation) was relatively low compared to the biases found for 1992 and 1994, and it was more evenly distributed over the different months, leading to a higher correlation coefficient (0.89). Only March, April, and May 1997 did not satisfy the criteria of reasonable agreement.

Monthly precipitation threat scores for thresholds varying from 0.1 to 3 mm day^{-1} are presented in Table 4. The threat scores are large (0.7–0.8) for light precipitation thresholds, and decreased with increasing rainfall amounts. The low scores of thresholds 2 mm day^{-1} and higher confirmed heavy precipitation months of 1992 that were missed. Since monthly precipitation was generally small in 1994, the trend is shifted toward lower threshold values, and missed precipitation already appeared at the threshold of 1 mm day^{-1}. The small sample size ($n < 10$) partly explained the null score obtained for 2 and 3 mm day^{-1} thresholds. Year 1997 had the best threat scores, with 0.42 as the lowest value, confirming the model's ability to reproduce the annual cycle of that wetter year. More detailed analysis was performed by spatially (Figs. 5–7) and temporally (Fig. 8) decomposing the precipitation series.

c. Monthly precipitation patterns

Considered station-by-station, the correlation coefficients (Table 2) were 0.64, 0.44, and 0.79 for 1992, 1994, and 1997, respectively. These correlation coefficients were similar to those found over the domain average, indicating that the spatial distribution of the annual cycle was generally well reproduced by the model or consistently biased. Figures 5–7 show the spatial distribution of the bias between simulated and observed monthly precipitation, linearly interpolated between the 35 rain gauge locations for 1992, 1994, and 1997, respectively. Four general features were identified: 1) small bias and little or no spatial structure; 2) joint presence of large negative and neighboring large positive bias; 3) spatial trend of bias over the domain; 4) substantial bias distributed throughout the domain. The first was a spatially homogeneous distributed bias, usu-

TABLE 3. Bias between simulated and observed monthly precipitation at the 35 rain gauge locations: mean bias (b; mm day^{-1}), mean relative bias (rb; %), and ratio between the mean absolute value of the bias and the standard deviation of observed monthly precipitation (b/σ).

	1992			1994			1997		
Month	b	rb	b/σ	b	rb	b/σ	b	rb	b/σ
Jan	0.24	>100	0.99	0.05	4	0.77	−0.95	−29	1.61
Feb	−0.20	−10	0.98	0.17	15	1.47	0.28	>100	1.03
Mar	−0.03	−4	0.62	0.06	66	0.80	0.23	>100	17.23
Apr	−0.07	−8	0.72	−0.27	−24	0.68	0.84	51	1.64
May	−0.09	−9	1.28	−0.94	−81	1.95	−1.07	−63	3.04
Jun	−1.46	−37	2.02	−0.08	−99	0.56	−0.12	−13	1.44
Jul	0.09	38	0.94	−0.05	−74	0.34	−0.26	−80	0.72
Aug	−0.03	−12	0.64	−0.02	−90	0.48	−0.69	−55	1.01
Sep	−0.57	−99	2.75	0.18	51	0.93	−0.86	−70	1.02
Oct	−2.50	−76	2.71	−1.31	−85	1.74	−0.44	−49	.099
Nov	0.22	>100	0.97	−0.67	−67	4.21	−0.27	−8	0.87
Dec	−0.01	−1	0.62	0.24	>100	1.02	−0.01	−0	0.79

TABLE 4. Monthly precipitation (P) threat scores for different precipitation thresholds (PT) in mm day^{-1}. The threat score for a given PT is defined as the number of $P >$ PT correctly simulated, divided by the sum of the number of observed $P >$ PT and the number of mistaken alarms (Wilks 1995). A mistaken alarm is a simulated event that was not observed. Threat scores vary between 0 (no simulation skill) and 1 (perfect simulation).

PT (mm day^{-1})	1992	1994	1997
0.1	0.71	0.80	0.77
0.25	0.70	0.57	0.72
0.5	0.75	0.51	0.65
1	0.59	0.35	0.60
1.5	0.56	0.07	0.64
2	0.37	0	0.67
3	0.19	0	0.42

ally close to zero, indicating general agreement between modeled and observed monthly rainfall, with the exception of one or two particular locations, creating one or two distinct patches of bias. The month of July 1994 best exemplifies this feature. Summer months were very dry, with some localized convective storms. In 1994, the model missed a few small storms (July) or underpredicted the amount of rain (August). In July 1997, the model missed storms in the eastern part of the domain. In addition to those summer months, April 1994 had a very good model to observation fit, except for three border stations. In September 1994, the model overestimated the precipitation in the northwest corner of the domain. In October 1997, the large discrepancy in the central-east part of the domain is quite unusual and cannot be explained easily. Thus, we suspect a possible measurement error.

The second general feature was identified as a pattern in the bias fields that indicated a spatial mismatch between observed and simulated rainfall fields. Stations with large negative biases are the locations where the model did not capture the convective storms, and correspondingly large positive differences indicate modeled storms that were not observed. A joint presence

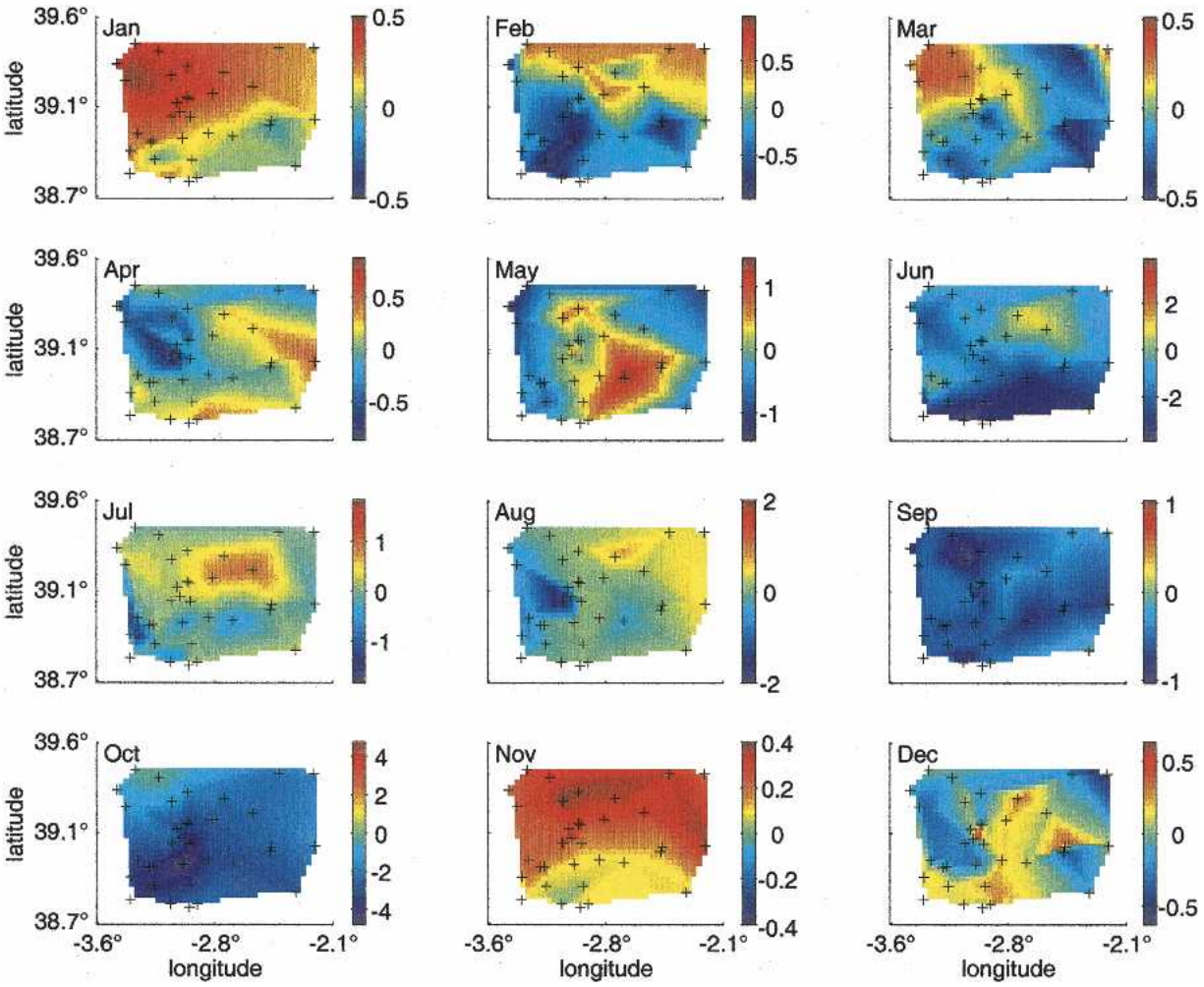

FIG. 5. Spatial linear interpolation of the bias between simulated and observed monthly precipitation at the rain gauge locations (crosses) for 1992.

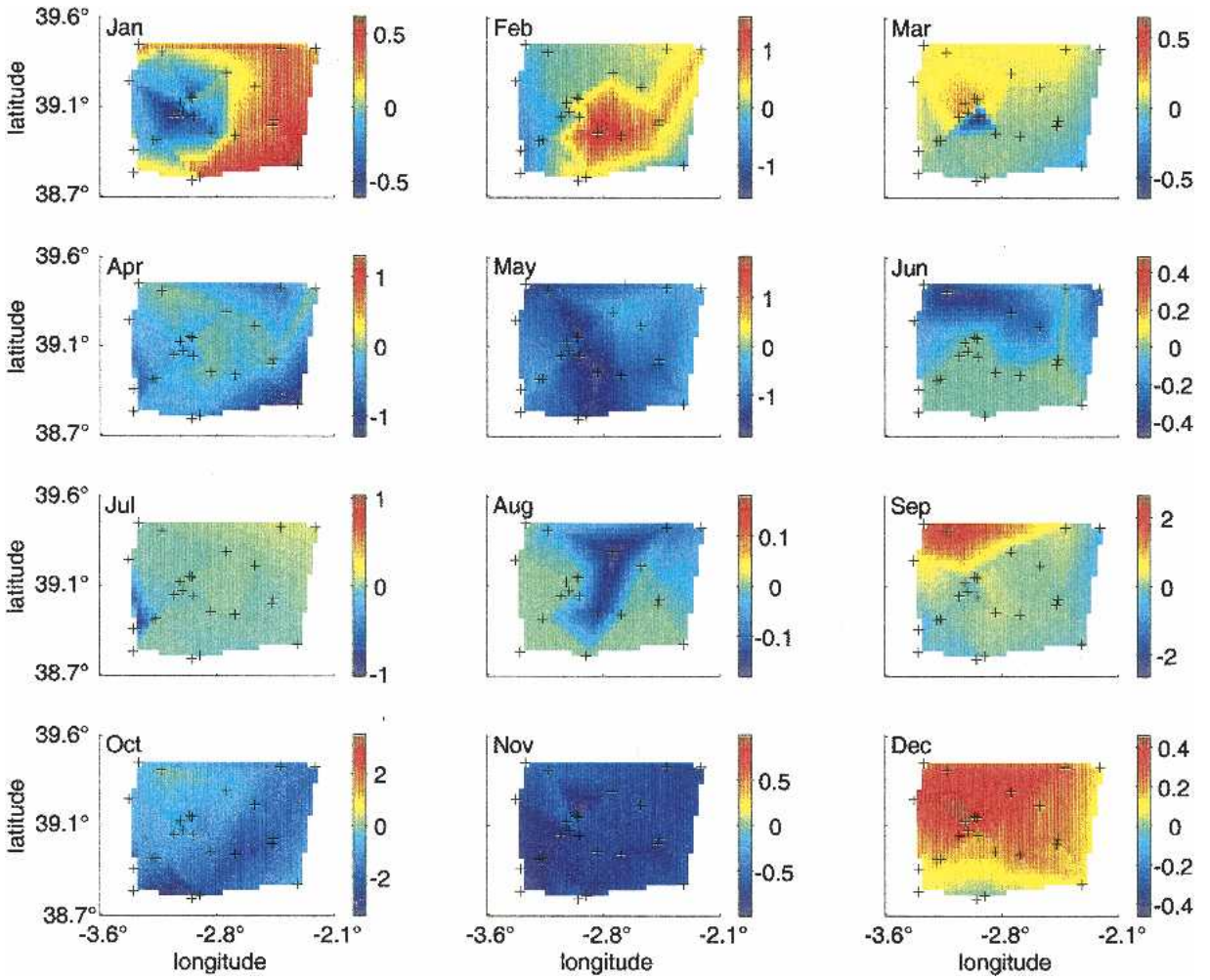

FIG. 6. Same as Fig. 5 but for 1994.

indicates a spatial shift between observed and simulated rainfall. Examples were found in July and August 1992 where the model shifted the storms northeastward, but matched the total rainfall amount. August 1997 had an eastward shift, March 1994 had a localized single storm event modeled slightly farther north than observed, and modeled precipitation in February 1994 centered all events at the same location while they were observed in two different locations. May 1997 had a similar pattern to that of February 1994. In conclusion, this scattered pattern type was indicative of convective storm events that the model was able to capture, with some errors in the spatial location or peak magnitude. Given the random nature of convection, this is not a serious concern.

The third feature combines cases in which a spatial trend in bias was detected. Most winter months belonged to this category. January, February, and November 1992, December 1994, and February and March 1997 showed a north–south trend with positive biases in the northern part. June 1994 had the reversed north–south trend, with the north being more negatively biased. January 1994 and December 1997 displayed a west–east trend, with increased bias toward the east. March 1992 had a northwest to southeast trend, while November 1997 had a southwest to northeast one, with both months having positive biases in the northern corner. This feature indicates displacement of the precipitation center for large-scale events, usually in addition to a mismatch of the peak amount. Figure 2 shows that the northern part of the domain is almost flat, with an important patch of semidesert in the western corner, while the south displays more topographic variability. Modeled winter rainfall was higher than observed in the mountain part, and lower in the flat semidesertic areas. Because most rain gauges were located in the flat area, or in the hilly part in the center of the domain, the southern mountainous area's overpredicted rainfall could be linked to a lack of representative observations. The model may also underestimate the northern semidesertic precipitation. Thus the typical north–south trend may be partly due to higher-elevation lack of

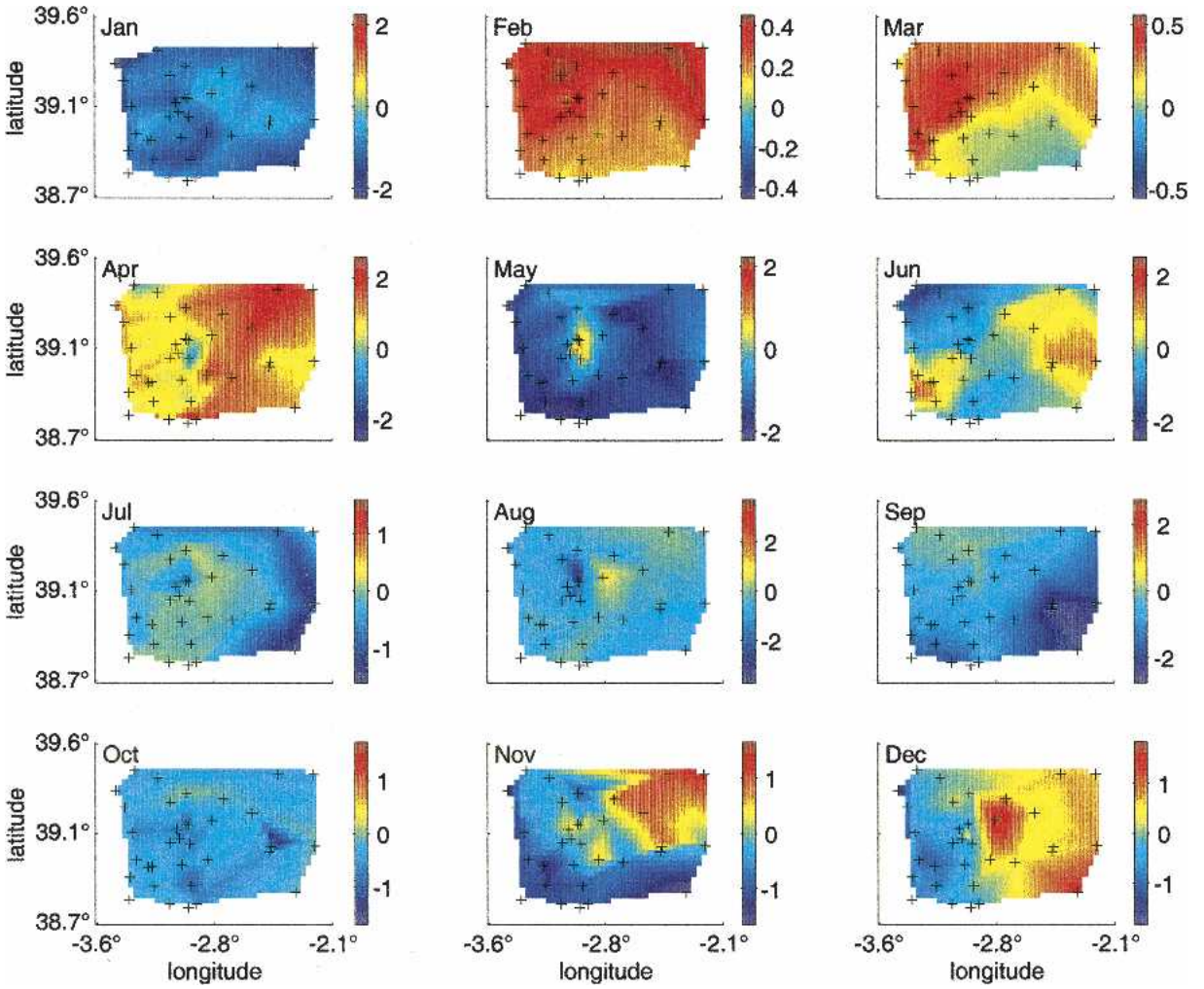

FIG. 7. Same as Fig. 5 but for 1997.

observation and/or higher-elevation modeled overestimation associated with a semidesert lower rainfall. Those joint elements shifted the center of the modeled precipitation southward compared to observations, with typical displacements of 20–30 km and about 0.3 mm day^{-1} in peak rainfall differences, both of which were small relative to the scale of the rainfall process and amount.

The last general feature was the existence of a substantial bias throughout the domain. The main reason for this was an overall underprediction of the precipitation. Months already identified as problematic, like June, September, and October 1992, May, October, and November 1994, and January and May 1997 belonged to this category. As emphasized later in section 5, general underprediction was likely linked to large-scale precipitation events that were influenced by the advected moisture entering the domain. Since the chosen domain size was small, the modeled variables were largely influenced by the lateral boundary conditions (Seth and Giorgi 1998; Pielke et al. 1999; Weaver et al. 2002). Thus, errors in atmospheric moisture boundary forcing could result in inaccurately modeled precipitation (Park and Droegemeier 2000). The monthly accumulated, domain-averaged precipitation differed significantly depending on the boundary forcing that largely defined the number of precipitation events in a month and their spatial extent. The problematic months involved precipitation covering a large fraction of the domain, with either high event frequency or large peak magnitude, identifying a potential weakness in the modeling approach due to sensitivity to atmospheric moisture boundary forcing. Another drawback of the modeling setup is the large resolution mismatch (about one order of magnitude) between the forcing data and the model mesh, which could lead to strong vertical motions and accumulated rainfall close to the boundaries, decreasing the atmospheric moisture advected through the domain. Analyses of the boundary cells (not shown) indicate that the model did not produce

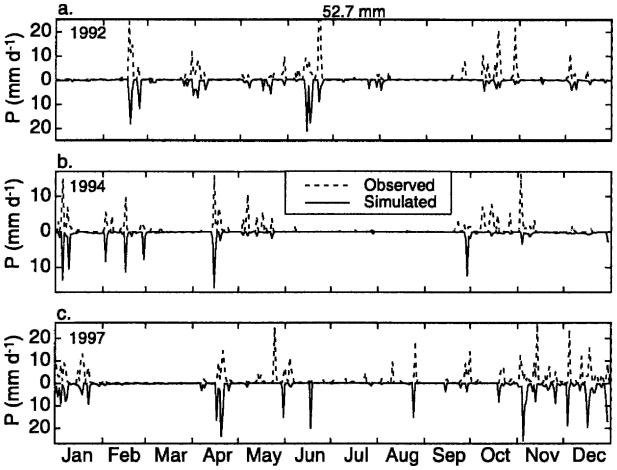

FIG. 8. Daily precipitation time series (mm day^{-1}) averaged for the 35 rain gauges (dotted line) and the corresponding 35 averaged 4-km-grid simulated values interpolated to the gauge location (solid line) for (a) 1992, (b) 1994, and (c) 1997. The simulated values are reversed in direction to improve visualization.

strong vertical motions nor excessive rainfall there. Exceptions were found for September 1992 and August and September 1997, where accumulated water in the southeastern corner of the coarse grid could possibly explain the underpredicted precipitation over the domain. The temporal distribution of rainfall events is analyzed in the next subsection, while the sensitivity of the model to the atmospheric moisture boundary forcing is discussed in more detail in section 5.

d. Daily precipitation analysis

As seen in the previous section, a few monthly mean precipitations were underpredicted by the model. The daily precipitation time series are used to further analyze this aspect of the simulations. Figure 8 shows the average value of the 35 rain gauges' daily-precipitation amounts and the corresponding average value of the simulated daily precipitation interpolated to the same 35 locations. In general, the model captured the timing of events and did not produce precipitation when none was observed. Some unobserved drizzle [and maybe unobservable due to gauges' undercatch of drizzle (Sevruk 1982)] was limited to winter months (November to April). While for some precipitation events, modeled and observed peaks agreed well, most were under- or overestimated, with an overall correlation of daily rainfall of only 0.35 ($n = 1096$). Few overestimates were simulated in late September 1994 and May and November 1997. The overestimated points arose from the model lumping rainfall into one event rather than distributing it over a series of days, as seen in the observations. As seen in the precipitation spatial distributions, summer months also had some storms that were completely absent in the model. June 1992 had a large precipitation event on the 22d, with intensities reaching 80 mm day^{-1} in the southern part of the domain (52.7 mm day^{-1} on average). Even if the model predicted a localized 35 mm day^{-1} peak over the southeastern part of the domain, the peak was largely underestimated, and the rainfall spatial extent was not simulated properly. Thus, the monthly underestimation was primarily linked to a single very large precipitation event. September 1992 had two precipitation periods, each consisting of isolated storms in a different part of the domain. While the model captured some isolated storms at the right location, the simulated value was an order of magnitude too low, compared to observations. October 1992 had three precipitation periods, with modeled values also being an order of magnitude smaller than observed. The same problem appeared in May and October 1994, while November 1994 had, as did June 1992, a single undercaptured peak event. April 1997 had an overestimated peak in the 5-day rainfall, while May 1997 had the same low magnitude problem found in September and October 1992 and May and October 1994. Overestimated peaks, as with April 1997 or February 1994, were likely due to convective precipitation, confirmed by the absence of strong horizontal winds entering the domain. This convective condition was also present in most of summer month—in September 1992 in particular—creating a situation in which a rain gauge could have caught a localized convective rain that was not representative of the region. Two other reasons explain the underestimated peaks. First, averaging smoothes peaks and precipitation at each model grid represents the averaged value of the entire grid cell. These averages were then further averaged by the interpolation process used for comparison with the gauge data. Also, boundary forcing is an additional likely source of the differences, as discussed in section 5.

5. Model sensitivity

The model evaluation showed a general underprediction of simulated rainfall compared to the observed values, with a few overestimated peaks. It is beyond the scope of this study to explore all possible sources of uncertainty in the model, and only the sources of atmospheric moisture content—a key variable in the precipitation process—are analyzed here. These sources in the domain are advection through the lateral boundaries and evapotranspiration.

a. Lateral boundary conditions

Given the proximity of the study domain to the lateral boundaries, atmospheric moisture prescribed there strongly influenced processes within the study domain. NCEP reanalysis data used for boundary forcing are known to have errors and uncertainties, especially in the moisture fields (Kalnay et al. 1996). When compared to the corresponding European Centre for Me-

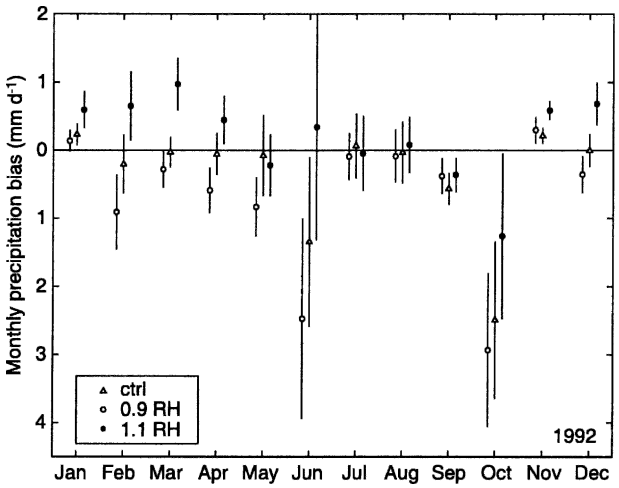

FIG. 9. Mean (symbols) and spatial standard deviation (bars) of the bias between simulated and observed monthly precipitation averaged over the 35 rain gauge locations, shown for the control run (white triangle), a 10% decrease in the atmospheric relative humidity (RH) run (white circles), and a 10% increase in the atmospheric relative humidity run (black circles).

dium-Range Weather Forecasts (ECMWF) dataset over the simulated domain, NCEP values showed a −2.6% dry mean bias in relative humidity, with [−10.7;5.8] % relative humidity as the interquartile range. The corresponding ECMWF to NCEP ratio represented 0.88 to 1.33 of the NCEP values. Given the relatively coarse spatial resolution (2.5° × 2.5° latitude–longitude) of the NCEP reanalysis dataset, few data points were used in creating the domain boundary conditions. Thus, the values of each NCEP point had a relatively large influence, as would their corresponding errors. To evaluate to what extent errors in atmospheric moisture data could propagate through the domain and affect the simulated precipitation, the entire NCEP relative humidity dataset was uniformly modified in time and space by ±10% of the original values (within the ECMWF–NCEP difference range). Figure 9, which presents the results of this sensitivity analysis, shows different features. First, in this region and for this model setup, RAMS was sensitive to the air moisture boundary conditions. Precipitation decreased up to 83% of the control absolute value for the case of a 10% decrease in NCEP relative humidity and increased to a maximum of 159% of the control absolute value for the case of a 10% increase in NCEP humidity. Second, the model was more sensitive to the increased, compared to decreased, relative humidity. This suggests that the modeled atmospheric moisture was close to rain/no-rain threshold conditions. Third, under convective conditions, the model was not, or only mildly, sensitive to the boundary forcing, due to weak advection. In some particular cases (May, July), the general trend of increased precipitation under increased atmospheric moisture was reversed, showing decreased precipitation with increased atmospheric moisture, and correspondingly increased precipitation for drier boundary forcing (September, November), probably due to the indirect effect of soil moisture on the atmospheric boundary layer. Indeed, precipitation leads to moister soils, decreasing the surface sensible heat flux to the atmosphere and, therefore, weakening the convection. On a few days, the model was sensitive to the convection strength and suppressed the precipitation. The opposite situation was found in the drier condition. Except for convective cases, changes in atmospheric moisture essentially modified the amount of water per precipitation event, without changing their timing. With increased relative humidity forcing, the amount of drizzle was also increased.

These two runs show that, as expected because of the small domain size, RAMS is sensitive to the boundary forcing of atmospheric moisture content, except in weak advective conditions.

b. Initial soil conditions

The other source of atmospheric moisture content is evapotranspiration. For a given land cover, the main driver for evapotranspiration is available soil moisture. Eltahir (1998) and Zheng and Eltahir (1998) showed the importance of soil moisture in rainfall patterns and demonstrated its positive feedback. To assess the response of simulated precipitation to the uncertainty in the initial and boundary soil conditions, two sets of simulations were performed. The first set focused on changing the initial soil moisture from 50% in the control run to 20% and 80% of saturation, uniformly distributed in both horizontal and vertical directions. The second set of four runs was performed to study the influence of soil texture on precipitation by changing it from a sandy clay loam soil in the control run to two extreme values (sand and clay) and two realistic texture types for the region (loam and silty clay loam), also uniformly horizontally and vertically distributed.

Figure 10 shows the small but consistent effect of soil moisture in winter months at the beginning of the run, decreasing to little effect by the end of the simulation year, as the soil moisture became similar between the simulations. This result is in accordance with previous findings on soil moisture persistence (Liu and Avissar 1999a,b; Schar et al. 1999; Hong and Pan 2000). Initial soil moisture had almost no effect on the dry summer months, but presented the largest sensitivity in some specific convective precipitation events of May and June. As seen for the lateral boundary condition experiments, changes in soil moisture impacted the partition of surface energy fluxes, which in turn changed the precipitation. The soil texture effect (not shown) was under 0.05 mm day^{-1} for loam and silty clay loam and reached a maximum of 0.1 mm day^{-1} in the sand case. The potential error made in the choice of soil texture and/or initial water content was smaller than 0.07 mm day^{-1} in any month, emphasizing lack of overall sensi-

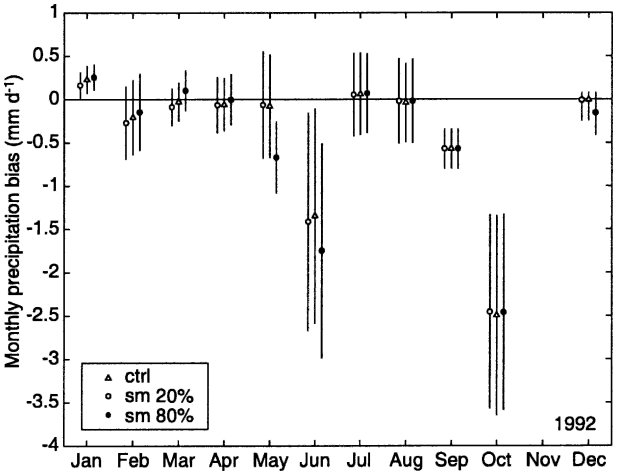

FIG. 10. Same as Fig. 9 but for 20% saturation initial soil moisture (white circles) and 80% saturation initial soil moisture (black circles).

tivity of the model to these parameters and/or the benefits of the spinup period.

Evapotranspiration is also linked to land-cover type. The modeled land cover was provided by the GLCC database, and in situ verification showed a good accuracy of the data. Based on prior studies performed with RAMS and other models (e.g., Weaver and Avissar 2001; Baidya Roy and Avissar 2002), we realize that this aspect of the model sensitivity is very important and is likely to have a significant impact on the model results. Because of the extensive number of simulations and analyses needed to cover this issue, we address it in a separate paper (N. Hasler and R. Avissar 2005, unpublished manuscript).

6. Summary and conclusions

In this paper, RAMS has been evaluated for a Mediterranean semiarid region, Castilla-La Mancha, central Spain, in a high (4 km) spatial resolution and long-term (1 yr) implementation. The model captured general spatiotemporal precipitation features, such as the timing of precipitation events and approximate location of storms. The domain-averaged monthly precipitation correlation between model and observations was 0.82. The threat scores were high (0.7–0.8) for low precipitation rates (0.1–0.25 mm day^{-1}) and decreased when increasing the precipitation rates, confirming the large biases found for large precipitation events, some of which associated with convective cells, which are random in nature. The unobservable model drizzle was low, and only present in winter months. The model showed a general negative bias toward observations, which was in general positively correlated with advected atmospheric moisture into the simulated domain. Since the model is quite sensitive to this forcing parameter, a small error in the forcing data induces a significant bias in the model results. This emphasizes the need for accurate lateral boundary conditions in this type of numerical experiment.

The small size of the domain led to a strong lateral constraint. High sensitivity to boundary forcing is a drawback of the chosen small domain size. While precipitation was sensitive to advected atmospheric moisture, additional test runs showed little influence of air temperature or winds on precipitation. Furthermore, simulated precipitation was barely affected in convective conditions. On the contrary, in these cases, as during May 1992, the aforementioned general positive correlation between atmospheric moisture and generated precipitation was reversed, and a drier atmosphere resulted in precipitation that was not present in the wetter case. This was due to the indirect effect of soil moisture, which modifies the surface energy fluxes' partitioning and, as a result, the structure of the atmospheric boundary layer. The model reacted to the available convective energy, which was insufficient in the wetter cases. Sensitivity to soil moisture confirmed this behavior. Hence, convective months were weakly influenced by the boundaries and sensitive to the surface conditions. Overall, the small size of the domain led to high sensitivity of the modeled precipitation only to boundary atmospheric moisture when large-scale precipitation occurred. The resolution mismatch between the forcing data and the model rarely produced boundary noise in vertical motion or precipitation patterns.

All sensitivity experiments presented here focused on testing the impact of different amounts of available atmospheric moisture in the simulated domain. To separate the influence of the boundary forcing from the internal variability of the model would require another set of experiments, such as those performed by other authors (e.g., Seth and Giorgi 1998; Takle et al. 1999; Christensen et al. 2001; Denis et al. 2002; Caya and Biner 2004), which is beyond the scope of this study. Some exploratory test runs with a larger domain over the Iberian Peninsula produced higher precipitation throughout the year. This could have been linked to the domain size, to the new boundary forcing located over the Atlantic and, as a result, the addition of the sea surface temperatures' impact, or to the modified topography by including the Spanish northern mountain ranges (Pyrenees, Cantabrian Mountains) in the model. Sensitivity to the surface conditions was kept to simple uniform-distribution cases. Preliminary results from ongoing sensitivity experiments to spatially varying conditions indicate that precipitation could be enhanced as compared to uniform cases, when the advection is weak.

In this study, RAMS was tested in a high-resolution climate mode, without explicitly assessing the influence of different model resolution. Comparison between the model runs with a single 16-km grid and the control runs showed that convective months were systemati-

cally better represented in the high-resolution simulation (control). The Kuo scheme in the 16-km setting dumped more water in convective rainfall than observed. Using the single 16-km grid only improved the simulated precipitation for 1 of the 36 months evaluated, namely, October 1994. This suggests that the simulated precipitation, for the specific domain and chosen setting, was improved by the higher-resolution nested grid.

This evaluation suggests that the RAMS modeling framework can be used as an investigation tool for studying land–atmosphere interactions over long time scales and at high resolution. The strong boundary forcing of a small domain remains a weakness for the large-scale advected precipitation systems, but does not affect the locally induced convective circulations. In the latter cases, the high-resolution setup clearly improves the simulation skills.

Acknowledgments. This research was supported by the National Oceanic and Atmospheric Administration (NOAA) under Grant GC01-101b. The views expressed herein are those of the authors and do not necessarily reflect the views of NOAA. Observation data were provided by the Instituto National de Meteorología, Madrid, Spain, with special thanks to Ernesto Rodriguez Camino. We are grateful to Anne Jochum and Joël Noilhan for sharing their soil data, and to Christopher A. Williams for editing the manuscript. We would like to acknowledge the contributions of the three anonymous referees whose comments and suggestions helped improve the original manuscript.

REFERENCES

Avissar, R., and R. A. Pielke, 1989: A parameterization of heterogeneous land surfaces for atmospheric numerical models and its impact on regional meteorology. *Mon. Wea. Rev.,* **117,** 2113–2136.

——, and M. M. Verstraete, 1990: The representation of continental surface processes in atmospheric models. *Rev. Geophys.,* **28,** 35–52.

Baidya Roy, S., and R. Avissar, 2002: Impact of land use/land cover change on regional hydrometeorology in Amazonia. *J. Geophys. Res.,* **107,** 8037, doi:10.1029/2000JD000266.

——, G. C. Hurtt, C. P. Weaver, and S. W. Pacala, 2003a: Impact of historical land cover change on the July climate of the United States. *J. Geophys. Res.,* **108,** 4793, doi:10.1029/2003JD003565.

——, C. P. Weaver, D. S. Nolan, and R. Avissar, 2003b: A preferred scale for landscape forced mesoscale circulations? *J. Geophys. Res.,* **108,** 8854, doi:10.1029/2002JD003097.

Betts, A. K., J. H. Ball, A. C. M. Beljaars, M. J. Miller, and P. A. Viterbo, 1996: The land surface–atmosphere interaction—A review based on observational and global modeling perspectives. *J. Geophys. Res.,* **101,** 7209–7225.

Bolle, H. J., and Coauthors, 1993: Efeda—European Field Experiment in a Desertification-Threatened Area. *Ann. Geophys., Atmos. Hydro. Space Sci.,* **11,** 173–189.

Braud, I., J. Noilhan, P. Bessemoulin, P. Mascart, R. Haverkamp, and M. Vauclin, 1993: Bare-ground surface heat and water exchanges under dry conditions— Observations and parameterization. *Bound.-Layer Meteor.,* **66,** 173–200.

——, R. Haverkamp, J. L. Arrúe, and M. V. López, 2003: Spatial variability of soil surface properties and consequences for the annual and monthly water balance of a semiarid environment (EFEDA experiment). *J. Hydrometeor.,* **4,** 121–137.

Bruce, J. P., and J. G. Potter, 1957: The accuracy of precipitation measurements. *Proc. Third National Meeting,* Toronto, ON, Canada, Royal Meteorological Society, Canadian Branch, 1–15.

Caya, D., and S. Biner, 2004: Internal variability of RCM simulations over an annual cycle. *Climate Dyn.,* **22,** 33–46.

Chen, C., and W. R. Cotton, 1987: The physics of the marine stratocumulus-capped mixed layer. *J. Atmos. Sci.,* **44,** 2951–2977.

Christensen, O. B., M. A. Gaertner, J. A. Prego, and J. Polcher, 2001: Internal variability of regional climate models. *Climate Dyn.,* **17,** 875–887.

Cotton, W. R., and Coauthors, 2003: RAMS 2001: Current status and future directions. *Meteor. Atmos. Phys.,* **82,** 5–29.

Davies, H. C., 1983: Limitations of some common lateral boundary schemes used in regional NWP models. *Mon. Wea. Rev.,* **111,** 1002–1012.

Denis, B., R. Laprise, D. Caya, and J. Cote, 2002: Downscaling ability of one-way nested regional climate models: The Big-Brother Experiment. *Climate Dyn.,* **18,** 627–646.

Dickinson, R. E., 1995: Land processes in climate models. *Remote Sens. Environ.,* **51,** 27–38.

——, and A. Henderson-Sellers, 1988: Modelling tropical deforestation: A study of GCM land-surface parameterizations. *Quart. J. Roy. Meteor. Soc.,* **114,** 439–462.

——, R. M. Errico, F. Giorgi, and G. T. Bates, 1989: A regional climate model for the western United-States. *Climatic Change,* **15,** 383–422.

Eltahir, E. A. B., 1998: A soil-moisture rainfall feedback mechanism. 1—Theory and observations. *Water Resour. Res.,* **34,** 765–776.

Gaertner, M. A., C. Fernandez, and M. Castro, 1993: A 2-dimensional simulation of the Iberian summer thermal low. *Mon. Wea. Rev.,* **121,** 2740–2756.

——, O. B. Christensen, J. A. Prego, J. Polcher, C. Gallardo, and M. Castro, 2001: The impact of deforestation on the hydrological cycle in the western Mediterranean: An ensemble study with two regional climate models. *Climate Dyn.,* **17,** 857–873.

Garcia de Pedraza, L., and A. Rieja Garrido, 1994: *Tiempo y clima en España, meteorología de las Autonomías (Weather and Climate in Spain, Regional Meteorology).* CIE Dossat 2000, 410 pp.

Giorgi, F., 1990: Simulation of regional climate using a limited area model nested in a general-circulation model. *J. Climate,* **3,** 941–963.

——, and G. T. Bates, 1989: The climatological skill of a regional model over complex terrain. *Mon. Wea. Rev.,* **117,** 2325–2347.

——, and L. O. Mearns, 1999: Introduction to special section: Regional climate modeling revisited. *J. Geophys. Res.,* **104,** 6335–6352.

——, G. T. Bates, and S. J. Nieman, 1993: The multiyear surface climatology of a regional atmospheric model over the western United States. *J. Climate,* **6,** 75–95.

Heck, P., D. Lüthi, H. Wernli, and C. Schär, 2001: Climate impacts of European-scale anthropogenic vegetation changes: A sensitivity study using a regional climate model. *J. Geophys. Res.,* **106,** 7817–7835.

Hong, S. Y., and H. L. Pan, 2000: Impact of soil moisture anomalies on seasonal, summertime circulation over North America in a Regional Climate Model. *J. Geophys. Res.,* **105,** 29 625–29 634.

Houghton, J. T., Y. Ding, D. J. Griggs, M. Noger, P. J. van der Linden, X. Dai, K. Maskell, and C. A. Johnson, Eds., 2001: *Climate Change 2001: The Scientific Basis.* Cambridge University Press, 881 pp.

Jochum, A. M., E. Rodríguez-Camino, H. A. R. de Bruin, and A. A. M. Holtslag, 2004: Performance of HIRLAM in a semi-arid heterogeneous region: Evaluation of the land surface and boundary layer description using EFEDA observations. *Mon. Wea. Rev.,* **132,** 2745–2760.

Jones, R. G., J. M. Murphy, and M. Noguer, 1995: Simulation of climate-change over Europe using a nested regional-climate model. 1. Assessment of control climate, including sensitivity to location of lateral boundaries. *Quart. J. Roy. Meteor. Soc.,* **121,** 1413–1449.

Kalnay, E., and Coauthors, 1996: The NCEP/NCAR 40-Year Reanalysis Project. *Bull. Amer. Meteor. Soc.,* **77,** 437–471.

Keyser, D., and R. A. Anthes, 1977: The applicability of a mixed-layer model of the planetary boundary layer to real-data forecasting. *Mon. Wea. Rev.,* **105,** 1351–1371.

Kuo, H. L., 1974: Further studies of the parameterization of the influence of cumulus convection on large-scale flow. *J. Atmos. Sci.,* **31,** 1232–1240.

Lee, T. J., 1992: The impact of vegetation on the atmospheric boundary layer and convective storms. Ph.D. dissertation thesis, Atmospheric Science Paper 509, Colorado State University, 137 pp.

Legates, D. R., and T. L. Deliberty, 1993: Precipitation measurement biases in the United-States. *Water. Resour. Bull.,* **29,** 855–861.

Liu, Y., and R. Avissar, 1999a: A study of persistence in the land–atmosphere system using a fourth-order analytical model. *J. Climate,* **12,** 2154–2168.

——, and ——, 1999b: A study of persistence in the land–atmosphere system using a general circulation model and observations. *J. Climate,* **12,** 2139–2153.

Louis, J. F., 1979: Parametric model of vertical eddy fluxes in the atmosphere. *Bound.-Layer Meteor.,* **17,** 187–202.

Marland, G., and Coauthors, 2003: The climatic impacts of land surface change and carbon management, and the implications for climate-change mitigation policy. *Climate Policy,* **3,** 149–157.

McCumber, M. C., and R. A. Pielke, 1981: Simulation of the effects of surface fluxes of heat and moisture in a mesoscale numerical model. 1. Soil layer. *J. Geophys. Res.,* **86,** 9920–9938.

Mellor, G. L., and T. Yamada, 1982: Development of a turbulence closure-model for geophysical fluid problems. *Rev. Geophys.,* **20,** 851–875.

Meyers, M. P., R. L. Walko, J. Y. Harrington, and W. R. Cotton, 1997: New RAMS cloud microphysics parameterization. Part II: The two-moment scheme. *Atmos. Res.,* **45,** 3–39.

Miao, J.-F., L. J. M. Kroon, J. Vilà-Guerau de Arellano, and A. A. M. Holstag, 2003: Impacts of topography and land degradation on the sea breeze over eastern Spain. *Meteor. Atmos. Phys.,* **84,** 157–170.

Molinari, J., 1985: A general form of the Kuo's cumulus parameterization. *Mon. Wea. Rev.,* **113,** 1411–1416.

Neff, E. L., 1977: How much rain does a rain gage gage? *J. Hydrol.,* **35,** 213–220.

Park, S. K., and K. K. Droegemeier, 2000: Sensitivity analysis of a 3D convective storm: Implications for variational data assimilation and forecast error. *Mon. Wea. Rev.,* **128,** 140–159.

Pielke, R. A., 2001: Influence of the spatial distribution of vegetation and soils on the prediction of cumulus convective rainfall. *Rev. Geophys.,* **39,** 151–177.

——, G. E. Liston, J. L. Eastman, L. X. Lu, and M. Coughenour, 1999: Seasonal weather prediction as an initial-value problem. *J. Geophys. Res.,* **104,** 19 463–19 479.

——, and Coauthors, 1992: A comprehensive meteorological modeling system—RAMS. *Meteor. Atmos. Phys.,* **49,** 69–91.

Reale, O., and J. Shukla, 2000: Modeling the effects of vegetation on Mediterranean climate during the Roman Classical Period: Part II. Model simulation. *Global Planet. Change,* **25,** 185–214.

Rodrigo, F. S., M. J. Esteban-Parra, D. Pozo-Vazquez, and Y. Castro-Diez, 1999: A 500-year precipitation record in southern Spain. *Int. J. Climatol.,* **19,** 1233–1253.

Romero, R., C. Ramis, and J. A. Guijarro, 1999: Daily rainfall patterns in the Spanish Mediterranean area: An objective classification. *Int. J. Climatol.,* **19,** 95–112.

Schar, C., D. Luthi, U. Beyerle, and E. Heise, 1999: The soil-precipitation feedback—A process study with a regional climate model. *J. Climate,* **12,** 722–741.

Segal, M., and R. Arritt, 1992: Nonclassical mesoscale circulations caused by surface sensible heat flux gradients. *Bull. Amer. Meteor. Soc.,* **73,** 1593–1604.

——, R. Avissar, M. C. McCumber, and R. A. Pielke, 1988: Evaluation of vegetation effects on the generation and modification of mesoscale circulations. *J. Atmos. Sci.,* **45,** 2268–2292.

Sellers, P. J., and Coauthors, 1997: Modeling the exchanges of energy, water, and carbon between continents and the atmosphere. *Science,* **275,** 502–509.

Seth, A., and F. Giorgi, 1998: The effects of domain choice on summer precipitation simulation and sensitivity in a regional climate model. *J. Climate,* **11,** 2698–2712.

Sevruk, B., 1982: Methods of correction for systematic error in point precipitation measurement for operational use. World Meteorological Organization Operational Hydrology Rep. 21, Publication 589, 91 pp.

Shukla, J., and Y. Mintz, 1982: Influence of land-surface evapotranspiration on the earth's climate. *Science,* **215,** 1498–1501.

Takle, E. S., and Coauthors, 1999: Project to Intercompare Regional Climate Simulations (Pircs)—Description and initial results. *J. Geophys. Res.,* **104,** 19 443–19 461.

Tremback, C. J., and R. Kessler, 1985: A surface temperature and moisture parameterization for use in mesoscale models. Preprints, *Seventh Conf. on Numerical Weather Prediction,* Montreal, PQ, Canada, Amer. Meteor. Soc., 355–358.

Walko, R. L., W. R. Cotton, M. P. Meyers, and J. Y. Harrington, 1995: New RAMS cloud microphysics parameterization. Part I: The single-moment scheme. *Atmos. Res.,* **38,** 29–62.

——, and Coauthors, 2000: Coupled atmosphere–biophysics–hydrology models for environmental modeling. *J. Appl. Meteor.,* **39,** 931–944.

Warner, T. T., R. A. Peterson, and R. E. Treadon, 1997: A tutorial on lateral boundary conditions as a basic and potentially serious limitation to regional numerical weather prediction. *Bull. Amer. Meteor. Soc.,* **78,** 2599–2617.

Weaver, C. P., and R. Avissar, 2001: Atmospheric disturbances caused by human modification of the landscape. *Bull. Amer. Meteor. Soc.,* **82,** 269–281.

——, S. Baidya Roy, and R. Avissar, 2002: Sensitivity of simulated mesoscale atmospheric circulations resulting from landscape heterogeneity to aspects of model configuration. *J. Geophys. Res.,* **107,** 8041, doi:10.1029/2001JD000376.

Werth, D., and R. Avissar, 2002: The local and global effects of Amazon deforestation. *J. Geophys. Res.,* **107,** 8087, doi:10.1029/2001JD000717.

Wilks, D. S., 1995: *Statistical Methods in the Atmospheric Sciences: An Introduction.* International Geophysics Series, Vol. 59, Academic Press, 467 pp.

Zheng, X. Y., and E. A. B. Eltahir, 1998: A soil moisture rainfall feedback mechanism. 2. Numerical experiments. *Water Resour. Res.,* **34,** 777–785.